

## Cumulative damage in RC frame buildings – The 2017 Mexico earthquake case

Leonardo M. Massone\*<sup>1</sup>, Diego Aceituno<sup>1</sup> and Julian Carrillo<sup>2</sup>

<sup>1</sup>University of Chile, Blanco Encalada 2002, Santiago, Chile

<sup>2</sup>Universidad Militar Nueva Granada, UMNG, Cra. 11, Bogotá, Colombia

(Received September 16, 2022, Revised November 15, 2022, Accepted November 17, 2022)

**Abstract.** The Puebla-Morelos Earthquake (Mw 7.1) occurred in Mexico in 2017 causing 44 buildings to collapse in Mexico City. This work evaluates the non-linear response of a 6-story reinforced concrete (RC) frame prototype model with masonry infill walls on upper floors. The prototype model was designed using provisions prescribed before 1985 and was subjected to seismic excitations recorded during the earthquakes of 1985 and 2017 in different places in Mexico City. The building response was assessed through a damage index (DI) that considers low-cycle fatigue of the steel reinforcement in columns of the first floor, where the steel was modeled including buckling as was observed in cases after the 2017 earthquake. Isocurves were generated with 72 seismic records in Mexico City representing the level of iso-demand on the structure. These isocurves were compared with the location of 16 collapsed (first-floor column failure) building cases consistent with the prototype model. The isocurves for a value greater than 1 demarcate the location where fatigue failure was expected, which is consistent with the location of 2 of the 16 cases studied. However, a slight increase in axial load (5%) or decrease in column cross-section (5%) had a significant detrimental effect on the cumulated damage, increasing the intensity of the isocurves and achieving congruence with 9 of the 16 cases, and having the other 7 cases less than 2 km away. Including column special detailing (tight stirrup spacing and confined concrete) was the variable with the greatest impact to control the cumulated damage, which was consistent with the absence of severe damage in buildings built in the 70s and 80s.

**Keywords:** cumulative damage; damage index; frame buildings; infill walls; low-cycle fatigue; Puebla-Morelos earthquake; reinforced concrete buildings; soft-story

### 1. Introduction

On September 19, 2017, an earthquake of magnitude Mw 7.1 occurred in the Puebla-Morelos area that caused a series of buildings in Mexico City to collapse. This event is registered as the second most devastating earthquake since 1985 in terms of economic losses and fatalities (Arteta *et al.* 2019). Several of the collapsed buildings (32 cases) were built before 1985 and also presented a structure based on a reinforced concrete (RC) frame with masonry infill walls on all floors (Galvis *et al.* 2020), but the first one (Fig. 1a), leaving columns prone to damage due to soft-first-story mechanism and poor detailing (Fig. 1b). The extensive seismic instrumentation present in Mexico City is favorable to study the seismic record impact in the location of damaged

---

\*Corresponding author, Professor, E-mail: lmassone@uchile.cl



Fig. 1 Typical structural damage - (a) collapsed building, (b-d) damaged columns

buildings. In Fig. 1a, it can be seen examples of buildings that suffered the collapse of all the columns of the first floor after the earthquake, causing the upper levels to descend. It is inferred that the collapse in these cases began and spread in the columns due to numerous observations such as the one in Fig. 1b, which represents other buildings that did not collapse but exhibited severe structural damage in the columns of the first floor, where buckling in the longitudinal reinforcement bars and the loss of the concrete cover and core were observed.

Regarding the seismic records, the only station that recorded both the 1985 and 2017 earthquake events on soft soil in Mexico City was SCT. In Fig. 2, it is observed the elastic displacement spectra, which assume a single degree of freedom linear oscillator response, for the 1985 and 2017 earthquakes in both directions for the SCT station. The response spectra are created using the Newmark-Hall linear acceleration method with  $\beta = 0.35$ ,  $\gamma = 0.5$  and a typical damping factor of 5%. Although the moment magnitudes of the 1985 and 2017 earthquakes were vastly different (Mw 8.1 in 1985 vs. Mw 7.1 in 2017), in Fig. 2, it is shown that the elastic displacement demands (Sd), between 0 and 1.5 seconds, were practically identical. This is interesting since that range of periods coincides with that of the buildings most affected by the 2017 earthquake.

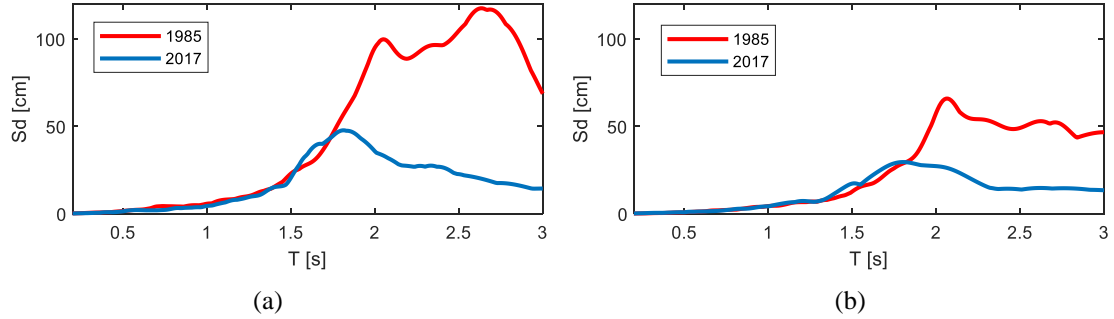


Fig. 2 Elastic displacement spectra of SCT station - (a) N90E, (b) N00E

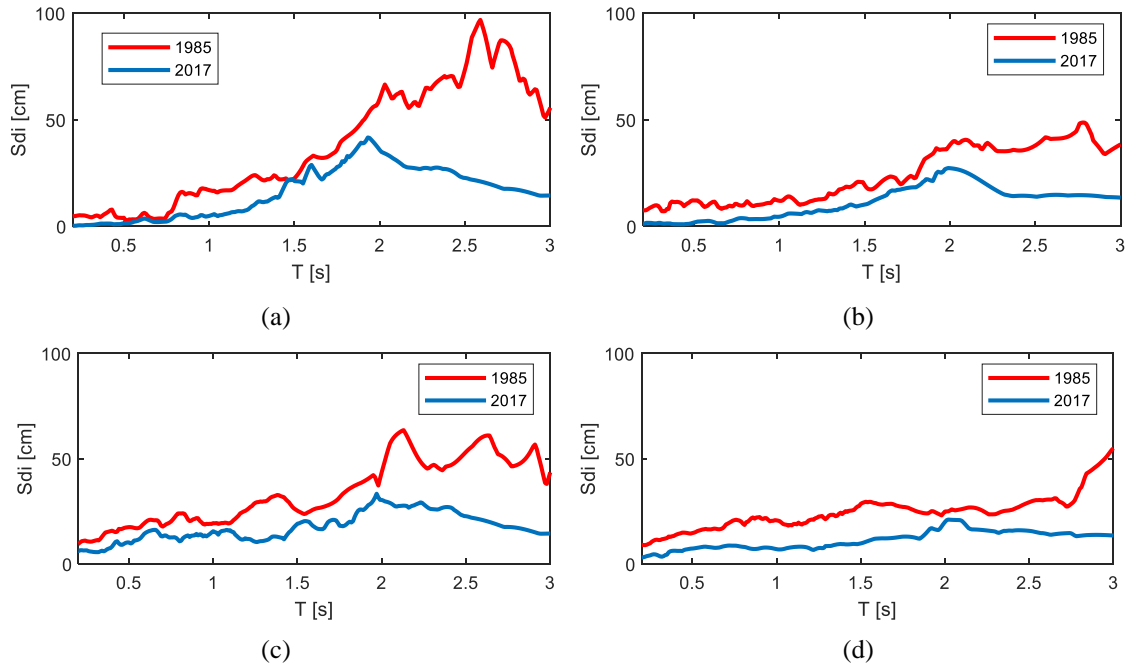


Fig. 3 Inelastic displacement spectra in directions - (a, c) N90E, (b, d) N00E, and (a, b)  $Q=2$ , (c, d)  $Q=4$

Since structures can fall into the non-linear range during an earthquake, a better representation of the displacement demand is considering an inelastic oscillator response. To fix the strength of the oscillator, a reduction factor  $Q$  is applied to the force obtained with the 1985 earthquake record under a linear response, that is, the oscillator strength depends on the elastic pseudo-acceleration spectra of the record reduced by a factor  $Q$ . Two  $Q$  factors are selected considering the typical values proposed in Mexican building codes: 2 and 4. A perfectly elastoplastic model with identical loading and unloading stiffness is used. Inelastic displacement spectra for the two  $Q$  values are presented in Fig. 3.

It is shown in Fig. 3 that for inelastic behavior, the displacement demand of the 1985 earthquake is markedly higher than that of the 2017 earthquake, even up to a period of 3 s. The trend is the same for both strength reduction factors ( $Q = 2$  and  $Q = 4$ ) and in both directions of

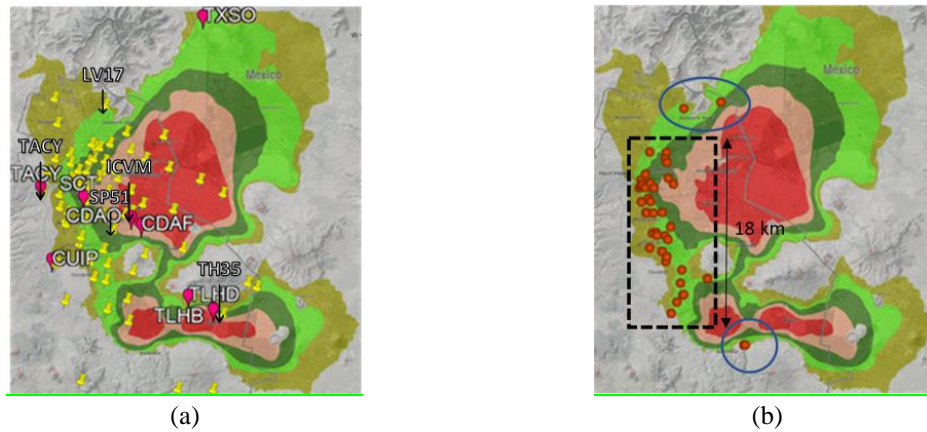


Fig. 4 Mexico City - (a) Seismic records, (b) Location of 44 collapsed buildings (after CDMX gov., 2017)

analysis. This motivates studying the cause of the collapse of buildings in 2017 that did not in 1985, considering that the 1985 displacement demands were higher than those in the 2017 earthquake. Damage associated with poor column detailing (confinement, lap splice) could result in early concrete crushing, bar buckling or shear failure, among others. However, such failure modes are associated with force or displacement threshold demands in the structures. Considering that the earthquake demand in the 1985 earthquake was similar or larger than the 2017 event, this type of failure, if possible, should have occurred during the 1985 event, and was not observed. Thus, with these simple observations, the hypothesis of the present investigation is that the damage observed, at least in part of the city, was a consequence of the damage accumulated mainly during the events of the 1985 and 2017 earthquakes, and not only due to the displacement demand of the 2017 earthquake, as is often thought (Rodríguez 2018). Previous studies have focused the attention on accumulated damage at global levels using energy and/or displacement demands (e.g., Rodríguez 2020). The present investigation uses a detailed structural model of a prototype building where damage due to fatigue is included at the longitudinal steel reinforcing level of the columns. Several analyses are performed to compare the response of the prototype under the isolated and combined actions of the 1985 and 2017 earthquakes, as well as the impact of variables such as the axial load, column size, longitudinal steel reinforcing ratio and transverse detailing. The behavior of the single degree of freedom system is also revised.

## 2. The Puebla-Morelos 2017 Mexico earthquake

### 2.1 Seismic stations of Mexico City in 2017

A collection of seismic records was obtained from the Center for Instrumentation and Seismic Records (CIRES), the Accelerographic Network of the Institute of Engineering at UNAM (RAII), and the Seismic Network of the Valley of Mexico (RSVM) (Quintanar *et al.* 2018). The map shown in Fig. 4a was constructed using this information, including the coverage of seismic stations in Mexico City during the 2017 earthquake (yellow markers). There are 58 CIRES records, 6 RAI records and 8 RSVM records delivering a total of 72 seismic records available and uniformly



Fig. 5 Collapsed buildings with a soft story - (a) before (Google maps 2017), (b) after (Google maps 2018) the 2017 earthquake

Table 1 Summary of selected collapsed buildings

Geographic coordinates	Collapse description	Construction year	# stories	$T(s)^*$
19.402328, -99.161378	Total collapse	1965	6	0.75
19.398972, -99.158926	Collapse of the ground floor	No info.	5	0.63
19.364923, -99.151864	Collapse of the ground floor	1960	5	0.63
19.422722, -99.139864	Total collapse	1960	5	0.63
19.360486, -99.140239	Collapse of the ground floor	1970	5	0.63
19.398652, -99.168763	Collapse of the ground/upper floor	1970	7	0.88
19.493407, -99.122896	Collapse of the facade. Severe wall damage	1960	7	0.88
19.387896, -99.146329	Total collapse	1960	5	0.63
19.304490, -99.123053	Total collapse	1960	6	0.75
19.366829, -99.156967	Total collapse	1965	7	0.88
19.348359, -99.145242	Severe damage of walls with diagonal cracks	1970	5	0.63
19.367567, -99.152837	Collapse of the ground floor	1970	5	0.63
19.412797, -99.171023	Total collapse	1960	8	1.01
19.373297, -99.137329	Total collapse	1970	4	0.50
19.387713, -99.163744	Total collapse	1960	6	0.82
19.387395, -99.163420	Total collapse	1970	8	1.09

\* Using the expression by Muriá and González (1995)

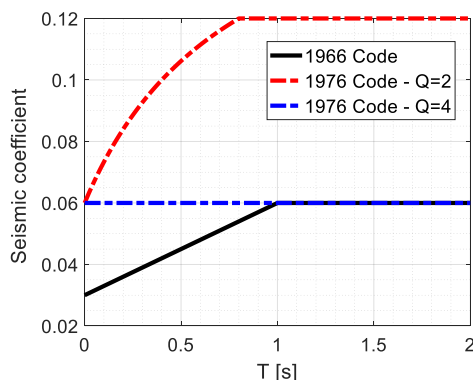


Fig. 6 Design spectrum prescribed in 1966 and 1976 codes

distributed in the urban area of the city. The data provided in this study were processed including the correction of the baseline, and the filtering of high and low frequencies with a low pass filter of 8th order with a frequency of 0.1 Hz and a high pass filter of 4th order with a frequency of 30 Hz, both of the Butterworth type.

## 2.2 Collapsed buildings

The location of the 44 collapsed buildings between 1 and 11 stories was concentrated in a fairly narrow strip that extends about 18 km in the NS direction of the west side of Mexico City, consistent with the location of soil II, IIIa and IIIb, with the largest presence in soil IIIa (light green in Fig. 4b), which may be related to local soil effects or other factors (Fig. 4b). Although there were 11 cases of 1 to 3-story low-rise buildings built with masonry walls, the range of most affected buildings was 4- to 8-story with a structure corresponding to flexible RC frames (16 cases) where the common characteristic was the soft first-story (columns with large spacing for car parking or circulation). The upper story usually presented infill masonry walls, increasing the strength and stiffness of such stories, and causing the displacement demands to be concentrated at the first story. These are the buildings and the failure mode under study in this work, and are described in Table 1. Fig. 5 shows 4 examples of collapses where the failure of the columns of the first story caused the descent of the upper body of the building. According to Rodriguez (2020), the buildings exhibiting significant damage or collapse in 2017 have not been retrofitted after previous earthquakes. The fundamental period of vibration (T), shown in Table 1, was estimated from the study by Muriá and González (1995), which defines a linear relationship,  $T = \alpha N$  in seconds, based on the number of floors (N) and the structural system of the building. The value of  $\alpha$  is 0.126 for RC frame systems on soft soil.

## 3. Building model and seismic records

### 3.1 Prototype building

The code that governs the design of buildings in Mexico City has been in a continuous process

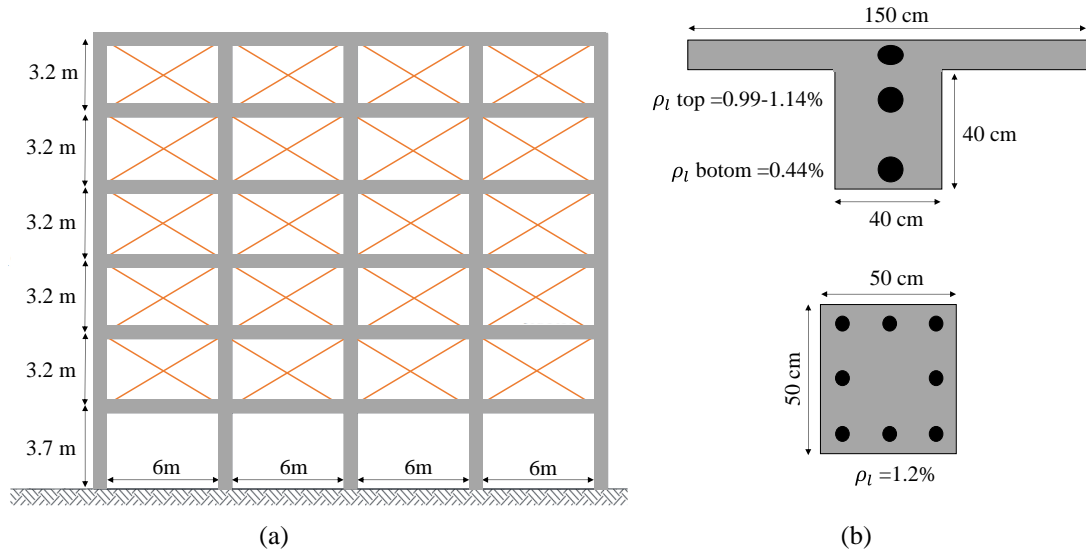


Fig. 7 Prototype model configuration – (a) general elevation, (b) beam-slab and column sections

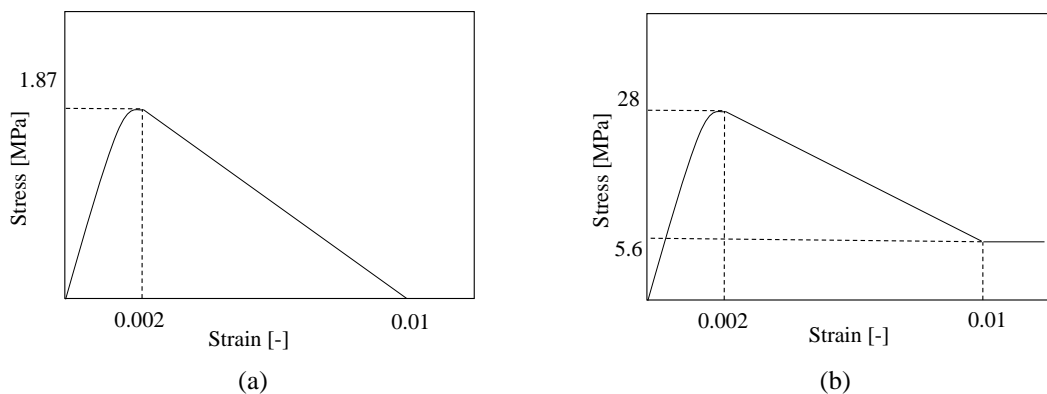


Fig. 8 Stress-strain model of materials - (a) masonry, (b) concrete

of updating. However, there are still many flexible structures built before 1985 that have low ductility capacity and were extremely damaged during the Puebla-Morelos earthquake in 2017. To explain the damage observed in these types of structures, Arteta *et al.* (2019) studied two sets of 6-story buildings based on RC moment frames each with different configurations of masonry infill walls, i.e., frames with totally or partially filled masonry walls. The first set of buildings was designed for low ductility (design strength reduction factor  $Q = 2$ ) and the second was designed for medium ductility ( $Q = 4$ ), according to all the requirements prescribed in the Mexico City Building Standards for Concrete Structures and for Seismic Design (NTC-C and NTC-S) of 1976, which regulated the structural design from 1976 to 1987 in Mexico City. The main difference between both sets is the implementation of special detailing provisions for  $Q = 4$  according to the NTC-C (NTC-C, 1976).

In this study, the date of construction of the collapsed studied buildings reveals that most of

them were built between the '60s and '70s, i.e., they were designed according to design requirements older than those prescribed in NTC of 1976 (NTC-C and NTC-S). A review of the Construction Regulations for Federal District (RCFD) of 1966 was carried out to compare the strength requirements of each design code. As shown in Fig. 6, the 1966 code considers a seismic strength coefficient (base shear as a fraction of the building weight) that linearly increases from 0.03 to 0.06 for a range of periods between 0 and 1 s, which is constant with a value of 0.06 afterward. Such a limit is identical to the seismic strength coefficient for the 1976 code for  $Q=4$ . Thus, it is considered that a prototype, based on the work by Arteta *et al.* (2019), for flexible RC frames with partially filled masonry walls designed in terms of required strength with  $Q=4$  is a well-representative model of the pre-1985 damaged buildings.

The height of the first floor of the prototype building (Arteta *et al.* 2019) is 3.7 m and 3.2 m for the upper floors, giving a total height of 19.7 m. There are three (3) and four (4) spans in the short and long directions, respectively, with a length of 6 m each. This gives a total floor area of 432 m<sup>2</sup>. For this work, this prototype is modeled in a 2D space (Fig. 7a) for the long direction (4 spans). The columns have a square section of 500 mm on each side. The beams are also square, but with a section of 400 mm on each side. In this case, the flexural contribution of the slab with a thickness of 100 mm and an effective width of 1.5 m was considered (Fig. 7b). In the case of masonry, it is a 100 mm thick wall and is located on the top 5 floors, composed of solid clay bricks, whose compressive strength is set at 7.0 MPa (Arteta *et al.* 2019).

All the reinforcement considered a yield strength  $f_y = 460$  MPa according to the average strength of 100 steel bars tested in Mexico City in 1993 (Rodríguez and Botero 1996). Likewise, the modulus of elasticity of steel reinforcement is set at 200,000 MPa until yielding is reached, from where strain hardening begins, whose slope is set at 1% of the elastic stiffness. The compressive strength of steel is reduced by 50% to include buckling effects given the observed slenderness ratio of buckled bars of about 24 (details are provided in section 4.1). The weight per floor including dead loads (which includes masonry fillings) is 7.7 kN/m<sup>2</sup>, with a total seismic weight of  $W = 6,621$  kN.

The beams of the prototype model consider the flexural contribution of the slab, with an upper longitudinal steel ratio ranging from 0.99% to 1.14% and a bottom longitudinal steel ratio of 0.44%. The columns of the first floor are configured to have a longitudinal steel ratio of 1.2%. The masonry walls were modeled with equivalent struts to account for the cracking of the walls. The width of each masonry strut was defined as 0.25 times the length of the wall diagonal (NTC, 2017). In Fig. 8, it is shown the stress-strain curves of masonry and concrete. According to experimental tests, confined masonry walls with an aspect ratio of 0.5, as in this case, fail by diagonal stress with a diagonal strength of  $\sqrt{f'_m} = 3.5 \text{ MPa} = 1.87 \text{ MPa}$  (Meli and Reyes 1971, similar results as with Massone and Ostoic, 2020), where  $f'_m$  is the compressive strength of masonry pile samples (Fig. 8a). Concrete was considered unconfined for columns and beams given the limited or nonexistent transverse detailing observed in old buildings. The unconfined concrete model contemplated a compressive strength of 28 MPa for a strain of 0.002 (Fig. 8b) (Arteta *et al.* 2019), with an ultimate deformation  $\varepsilon_u = 0.01$  for a residual stress of  $0.2f_c$  (Welt *et al.* 2017).

The numerical analyses in this study were performed in OpenSees (McKenna *et al.* 2000), including second-order P- $\Delta$  effects. The columns are modeled with displacement-based elements on the edges ( $L = 480$  mm) with 2 integration points, for better convergence, and a force-based element with 6 integration points in the central portion to avoid a finer discretization. The formulation was selected given that strain concentration was observed in the column ends within a length of 480 mm (Fig. 1b) due to the poor detailing that resulted in bar buckling within several

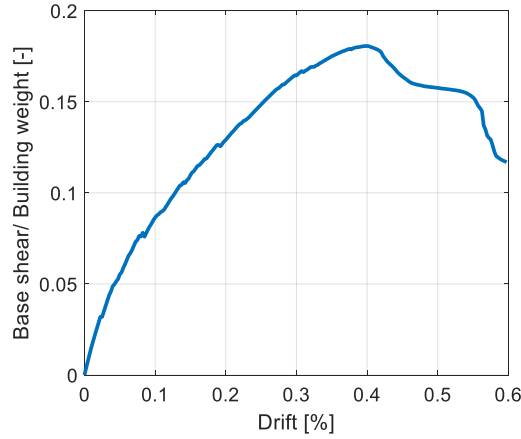


Fig. 9 Prototype pushover analysis – normalized base shear versus lateral displacement

stirrups. Thus, the displacement-based model allows for a linear curvature distribution where strains are concentrated, capturing the damage localization in concrete and steel reinforcement. The beams are modeled with force-based elements, with 2 elements at beam edges of 1.35 m and an additional central element. All beam elements considered 3 integration points.

In Fig. 9, it is shown the pushover analysis results for a lateral load pattern with the shape of the first fundamental mode, revealing the overall base shear versus the lateral top displacement of the prototype building. It is shown a strength degradation that starts at a 0.4% drift, which corresponds to 80 mm. The degradation of the strength by 20% is reached at about 0.5% drift, that is 100 mm. The maximum strength is  $\sim 0.18W$  (18% of the building weight), indicating that an over-strength of  $\Omega = 3$  is expected since the design strength is  $0.06W$  for a period of vibration with cracked sections ( $T_{cr}$ ) of 1.0 s (Fig. 6).

The fundamental period of vibration ( $T_0$ ) of the prototype model, after applying the gravitational load, is 0.6 seconds. The cracked period ( $T_{cr}$ ) was estimated according to FEMA 356 (2000), as  $T_{cr} = T_0 \sqrt{K_i/K_e}$ , where  $K_i$  and  $K_e$  are the initial stiffness and the stiffness at  $0.6V_y$  (60% of the yield lateral force, assumed as 60% of the lateral strength), respectively. From Fig. 9, the coefficient  $\sqrt{K_i/K_e} = \sqrt{\left(\frac{0.02W}{0.011\%}\right) / \left(\frac{0.11W}{0.15\%}\right)} = 1.6$ , which yields  $T_{cr} = 1.0$  s.

### 3.2 Model scheme validation

To validate that the modeling scheme, the material model, and the discretization criteria of columns, were good enough to capture the history response of main variables such as moment, shear and lateral displacement with a flexural failure mode, a specimen (M1) from the work by Jiménez and Massone (2018) is studied. As shown in Fig. 10, this work focuses on studying the seismic response of an RC cantilever wall with 5 stories, accounting for 5 vibration modes due to the seismic weight distribution. The weight was consistent with an axial load of  $0.07Agf^c$ . The wall is 2.15 m high with a cross-section of 150 mm  $\times$  40 mm, and the longitudinal boundary reinforcement is characterized by  $2\phi$ -6 mm bonded steel bars on each side. For transverse reinforcement,  $\phi$ 4 mm stirrups separated at 40 mm were placed at the wall bottom to provide

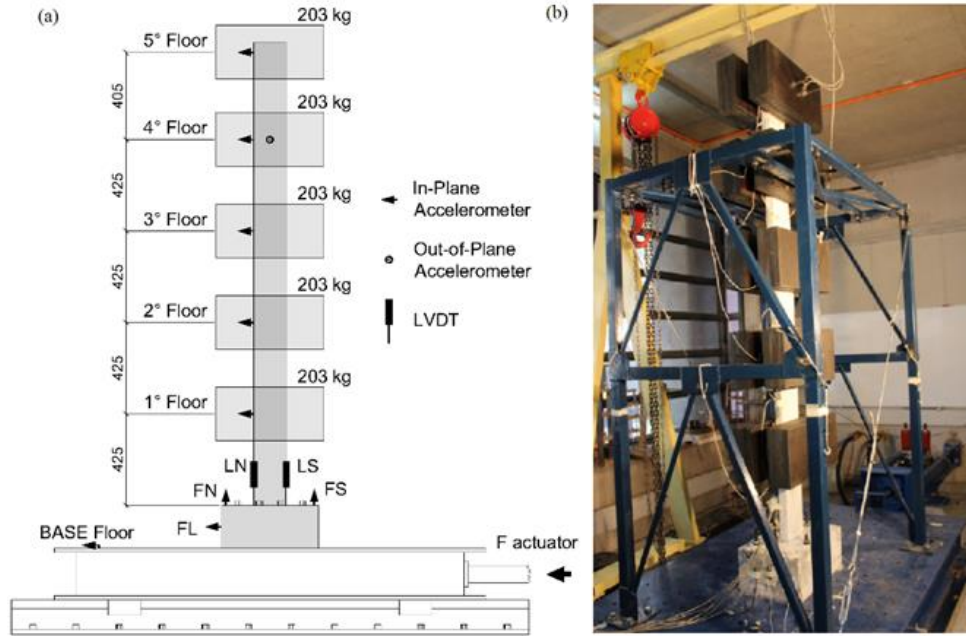


Fig. 10 Test setup of model validation (Jiménez and Massone 2018)

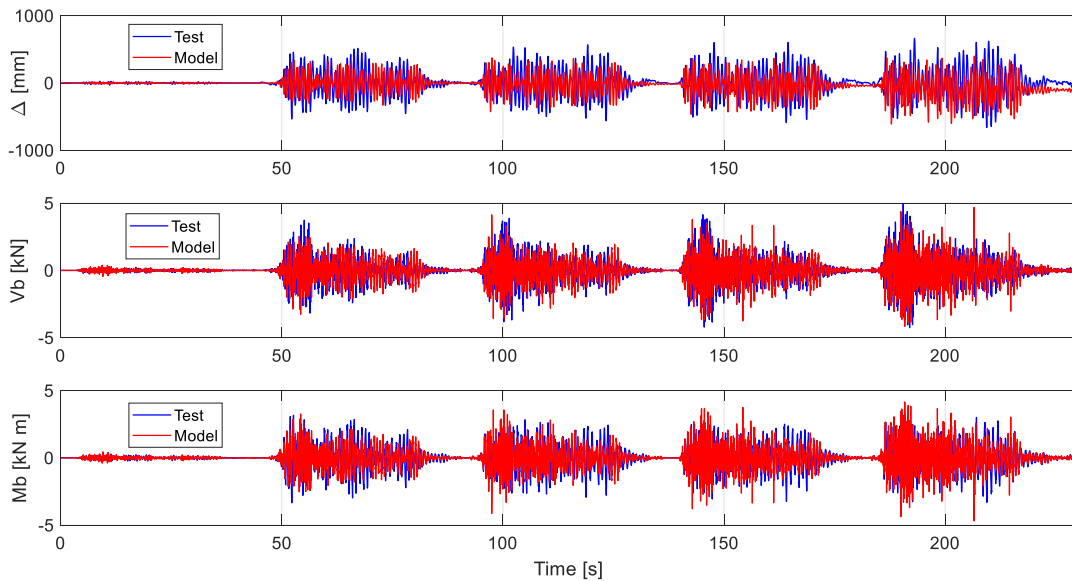


Fig. 11 Test validation - (a) top lateral displacement, (b) base shear and (c) base moment

confinement to concrete and lateral support to longitudinal bars. The yield strength for the steel was measured as 387 MPa and for the compressive strength of concrete was 42 MPa. The seismic records were applied at the base of the wall with a shake table corresponding to the Constitution record from the 2010 Chile earthquake scaled to 10% (C010), 100% (C100), 130% (C130), 150%

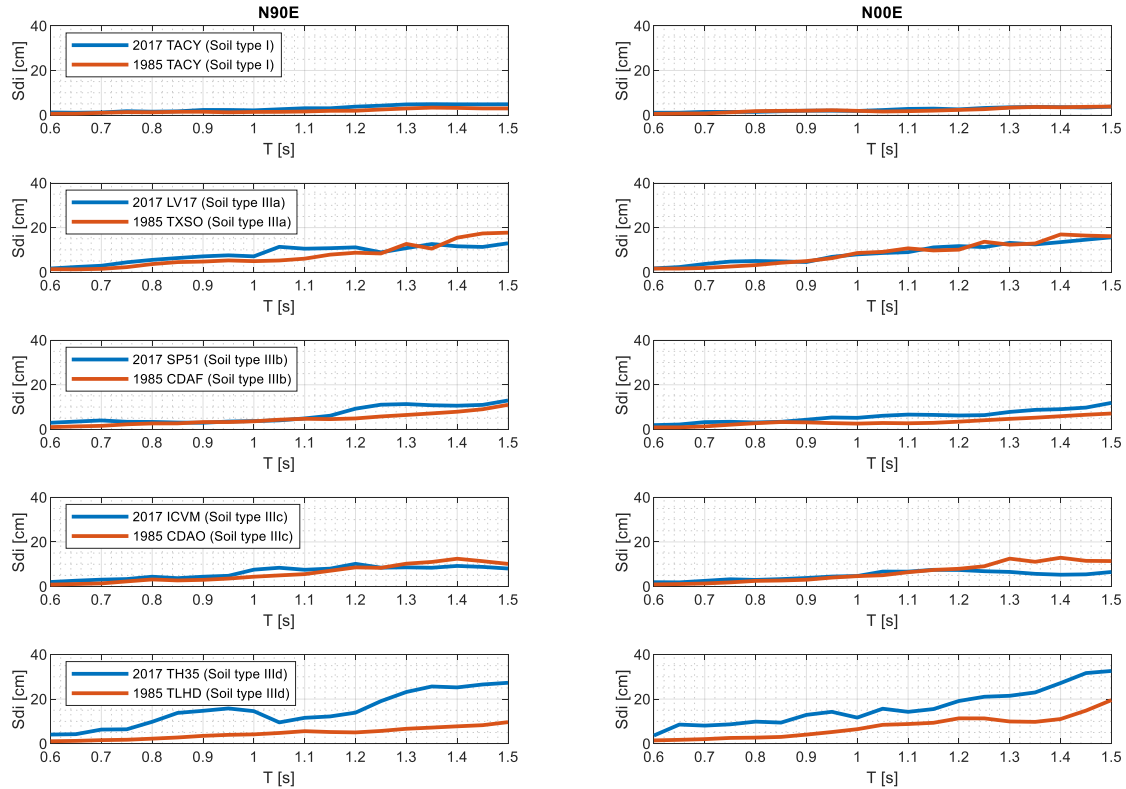


Fig. 12 Comparison of inelastic ( $\Omega=3$ ) displacement demands for close stations for the 1985 and 2017 earthquakes – (a) TACY, (b) TXSO, (c) CDAF, (d) CDAO, (e) TLHD

(C150) and 200% (C200), simulating damage in Chilean buildings (Massone *et al.* 2021).

The damage to the specimen was concentrated at the base of the wall mainly due to bending (Jiménez and Massone 2018). The experimental fundamental period of the wall was 0.37 s, as same as the model accounting for unintended cracking of the specimen due to transportation and shrinkage before testing. The moment, shear and top displacement distribution are relatively similar between the model and the experimental measurement (Fig. 11), with differences of less than 10% for the maximum displacement and shear, validating the modeling scheme used for the prototype.

### 3.3 Seismic demands of 1985 and 2017 earthquakes

In Fig. 4a, it is shown, with pink balloons, the location of the 8 seismic stations available in Mexico City that recorded the 1985 earthquake; two of them located on soil type I (CUP5 and TACY stations), one located on soil type IIIa (TXSO station), three on soil type IIIb (CDAF, SCT and TLHD stations), one on soil type IIIc (CDAO station) and one located on soil type IIId (TLHB station). Three of these stations also recorded the 2017 earthquake (SCT, TACY, CUP5), in addition to a series (69) of new stations that have only recorded the 2017 earthquake.

In Fig. 12, it is shown the inelastic displacement spectra (Sdi) based on the strength design of

the 1966 design code for frame buildings with flat slabs (Fig. 6), with an over-strength value of  $\Omega = 3$ , consistent with the over-strength observed in the prototype building. For each of these 5 stations that only recorded the 1985 earthquake, the closest stations with the 2017 record available and located on the same type of soil are identified (TACY for TACY, LV17 for TXSO, SP51 for CDAF, ICVM for CDAO, TH35 for TLHD) to compare their inelastic displacement demands ( $S_{di}$ ). The inelastic displacement demands are congruent with values lower than 100 mm for the fundamental cracked period of 1 s, with similar displacement demands for the 1985 and 2017 earthquakes, interchanging slightly larger values between them, except for the last case (TLHD station) where the demands exceeded this value, with magnitudes larger on the 2017 records than on the 1985 records. This suggests that the damage to the buildings may have been triggered by a mix between displacement demand and cumulative damage.

For the present study, a representative station of the 1985 records will be considered for each type of soil. For soil type I, the record of the CUIP5 station is chosen. Soil types II and IIIa will be represented by the records of the TXSO station, which is considered representative of the Transition Zone (Mayoral *et al.* 2016). The records from the SCT station will be representative of soil type IIIb, which is more conservative than using CDAF or TLHD stations. Soil types IIIc and IIId will be characterized with their only seismic record available from the CDAO and TLHB stations, respectively.

#### 4. Dynamic analysis and cumulative damage

For the nonlinear dynamic analysis, Rayleigh damping was defined as proportional to the mass and initial stiffness, with a damping value of  $\zeta = 5\%$  for the first and second vibration modes of the model. The defined damping value is consistent with values measured in frames with masonry infill walls (Ozkaynak *et al.* 2014). The KrylovNewton algorithm was used with the Newmark integrator with  $\gamma = 0.5$  and  $\beta = 0.35$ .

##### 4.1 Low-cycle fatigue and bar buckling

Seismic loading on structures imposes tensile/compressive cyclic strain demands in steel reinforcement of columns, walls, or other structural elements. When the demand is high enough, the structure can endeavor once or several times into plastic response causing permanent damage. The accumulation of large strain cycles can lead to a premature failure of reinforcing bars with a relatively small number of cycles, which is known as low-cycle fatigue damage. On the other hand, fatigue tests under low-stress levels can reach millions of cycles (e.g., Kwak and Park, 2001; Li *et al.* 2015). In reinforced concrete structures designed to predominantly respond in flexure during a seismic event, their ultimate failure is primarily associated with either fracture of reinforcing bars due to accumulation of low-cycle fatigue damage and/or buckling of reinforcing bars or crushing of concrete (Tripathi *et al.* 2018, Massone and Herrera 2019).

A simple method to predict the fatigue life of steel reinforcing bars including bar buckling was presented by Tripathi *et al.* (2018). The proposed model allows estimating the cyclic capacity of reinforcing bars in terms of the number of half-cycles needed to reach failure at a certain level of total strain amplitude. In that study, the buckling of a reinforcing bar is known to depend on its yield strength ( $f_y$  [MPa]) and slenderness ratio ( $L/D$ ), and its behavior can be defined by using a

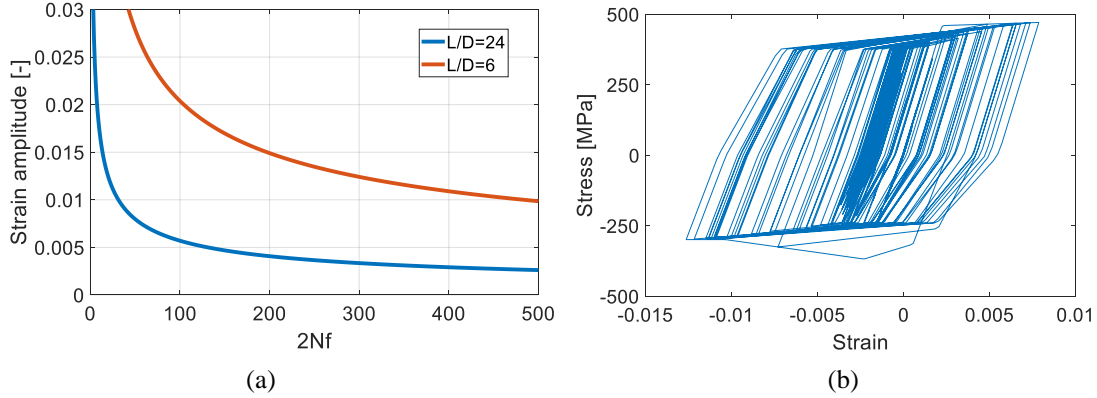


Fig. 13 Reinforcing bars - (a) low-cycle fatigue life, (b) stress-strain response in the prototype building

non-dimensional buckling parameter ( $\lambda$ ) that is computed as  $\lambda = \frac{L}{D} \sqrt{\frac{f_y}{100}}$ , where the slenderness ratio ( $L/D$ ) is the ratio of the unsupported length (i.e., buckling length,  $L$ ) to the diameter ( $D$ ) of the bar. Observations suggest that an increase in the slenderness ratio of the reinforcing bars results in a substantial reduction of their low-cycle fatigue life (Tripathi *et al.* 2018). Therefore, the low-cycle fatigue life of reinforcing bars can be evaluated using total strain amplitude ( $\varepsilon_a$ ), which is the average value between positive and negative strain levels, given by Eq. (1).

$$\varepsilon_a = \beta_0 (2Nf)^a \quad (1)$$

where  $\beta_0$  is the fatigue ductility coefficient and  $a$  is the fatigue ductility exponent, which can be calibrated using experimental test results, and  $Nf$  is the number of cycles to fracture. The low-cycle fatigue life of Grade 300E and 500E reinforcing bars was evaluated by testing specimens subjected to constant axial strain loading with amplitude ranging from 1% to 5% and different slenderness ratios. The calibration resulted in the coefficient values  $a = -\left(\frac{\lambda}{1200} + 0.441\right)$  and  $\beta_0 = \frac{-\lambda}{350} + 0.2$  for ductility fatigue exponent and coefficient, respectively (Tripathi *et al.* 2018).

The buckling length of the reinforcement observed after the Puebla-Morelos earthquake is approximately 480 mm for bars with a diameter of about 20 mm (Fig. 1b), which suggests a slenderness factor  $L/D \sim 24$  that was commonly observed in Mexico City after the earthquake. The buckling length has been validated in this study using the approach by Dhakal and Maekawa (2002), where the numerical model indicates that global buckling would be achieved by the longitudinal reinforcement under mode 2 (Massone and López, 2014) for 8 longitudinal bars (2 in each corner) equivalent to a reinforcement ratio of 1.2% and stirrups No. 2 (6.4 mm diameter) at 230 mm spacing (0.5d, where  $d$  is the distance to the tensile reinforcement), which is the maximum spacing allowed by the 1966 Mexican design code (NCR, 1966). That is, instead of observing longitudinal bar buckling between 2 consecutive stirrups (mode 1 – local buckling,  $L/D = 230/20 \sim 12$ ), buckling would be observed within 2 spacings. This is mainly caused by the small stirrup diameter, which is consistent with Fig. 1b. Thus, the actual buckling length to diameter ratio would be  $L/D \sim 24$  for mode 2, which was also inferred from the figure.

The strength of steel was defined as  $f_y = 483$  MPa on the prototype model with a life cycle of reinforcing bars considering a slender ratio of  $L/D = 24$  based on Eq. (1). For comparison

purposes, Fig. 13a shows the number of half-cycles ( $2N_f$ ) necessary to reach the fatigue failure for different strain amplitude levels and for slenderness ratio  $L/D = 6$  and  $24$ . The  $L/D = 6$  curve is also shown to compare with a case where special detailing is provided to columns, constraining the potential buckling length of longitudinal bars as 6 times the bar diameter, as it is required by codes as ACI 318-19 (2019) for Grade 60 steel.

The behavior of the steel for the prototype model is defined with an asymmetric behavior in tension and compression in OpenSees. This is done to incorporate the effects of strength loss in compression due to the buckling phenomenon of the longitudinal bars. A 50% strength loss in compression is estimated for the steel bars after the first cycle for a 1% amplitude strain and a slenderness  $L/D = 24$ , based on the work by Massone and Moroder (2009). Thus, the peak compressive stress at yielding was set as  $f_y = 460$  MPa, and the post-peak slope (negative) was set to reach a stress of  $0.5f_y$  at 1% strain. In Fig. 13b, it is illustrated the behavior of the prototype model steel in the central bottom column ( $L/D = 24$ ) for the SCT station considering the 1985 and 2017 seismic records.

#### 4.2 Damage counting

The expected behavior of the case-study building is assessed by inelastic analyses considering static and dynamic loading effects. As mentioned before, there are 72 seismic records available, uniformly distributed over Mexico City. Both directions N90E and N00E are evaluated independently so that a total of 144 dynamic analyses were performed per case. Each one considers a single seismic record of 1985, followed by a single seismic record of 2017, in the cases that both events are considered.

The main results from the dynamic response of the prototype building subjected to SCT records in the N90E direction are shown in this section to explain the methodology used to calculate the damage index considering the low-cycle fatigue life model of reinforcing bars. The first step is to obtain the cyclic stress-strain response of reinforcing bars (modeled as fibers, Fig. 13b) for columns on the first floor since larger cyclic demands are concentrated there in comparison with the upper-floor columns. In Fig. 14, it is shown the strain-time history for the values obtained for the bottom central column (Fig. 13b). The first 240 seconds of the response correspond to the 1985 record, followed by the 2017 record.

As shown in Fig. 14, a maximum strain value above 0.01 is reached, although several cycles barely reach yielding. The fatigue damage is calculated based on rain-flow counting (Downing and Socie 1982). Thus, peak strains must be identified for the estimation of the total strain amplitude of each half-cycle. Half of every absolute difference between one peak and an adjacent one is named  $\epsilon_a$  or total strain. The low-cycle fatigue life model proposed by Tripathi *et al.* (2018) is introduced to count damage from each half-cycle ( $D_i$ ). This quantity is defined in Eq. (2), following Eq. (1) which defines the cyclic capacity of reinforcing bars. The absolute damage index (DI) is calculated as the sum of all terms using Eq. (3). With those considerations, the progression of accumulated damage in time can be also plotted as in Fig. 15. For comparison purposes, the prototype model is also run for a special detailing of transverse reinforcement in columns with slenderness ratio  $L/D = 6$  (reinforcing bar without buckling and confined core concrete), showing how the damage is largely reduced given in part due to the larger fatigue life (Fig. 13a).

$$D_i = \left( \frac{1}{2Nf} \right)_i = \left( \frac{\epsilon_a}{\beta_0} \right)_i^{1/a} \quad (2)$$

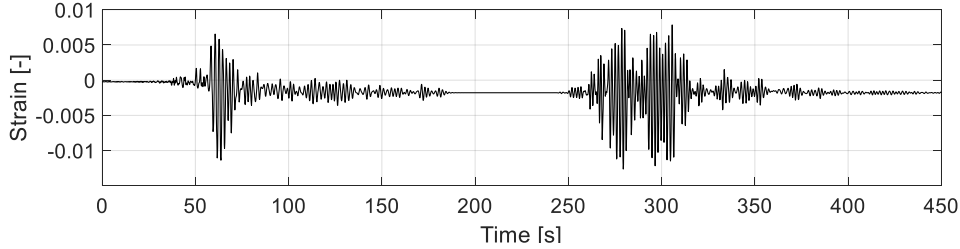


Fig. 14 Cyclic strain-time history of a reinforcing bar (central bottom column) in the prototype building.

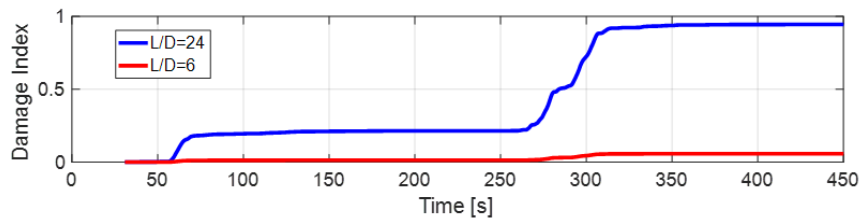


Fig. 15 Time history of damage index progression for a reinforcing bar of the central bottom column

$$DI = \sum_i D_i = \sum_i \left( \frac{\varepsilon_a}{\beta_0} \right)_i^{1/a} \quad (3)$$

## 5. Prototype and SDOF model results

### 5.1 Low-cycle fatigue in the prototype model

The seismic behavior of the prototype model is evaluated in all the stations that registered the 2017 earthquake. After running the non-linear dynamic analysis for the prototype, the accumulated fatigue damage model is applied in the most strained bar in the columns, defining a damage index per location (station) and direction of analysis. With the damage index results of each seismic station, an interpolation of the data on the geographical surface is performed to create isocurves that define the same level of damage or fatigue damage index in the city. This process is called Kriging (Matlab 2020), and it is done by weighting the known data according to the distance to the interpolated point.

In Fig. 16, it is shown the isocurves of the fatigue damage index (DI), which considers the direction of the largest demand in each station for the 1985 records (Fig. 16a) and the combined 1985 and 2017 records (Fig. 16b). The color scale classifies the intensity of the damage index of each isocurve in the map, limited by geographic coordinates. The red dots are the locations of the 16 collapsed buildings of the study group, whose structure, year of construction and failure mode closely match that of the prototype model. Stations with  $DI > 1$  are marked with their corresponding value. The action of the 1985 earthquake generated an accumulation of damage of about 20% with respect to the total required damage to reach the fracture of the steel reinforcement (Fig. 16a). This accumulation of damage is concentrated in the northern part of the city, and

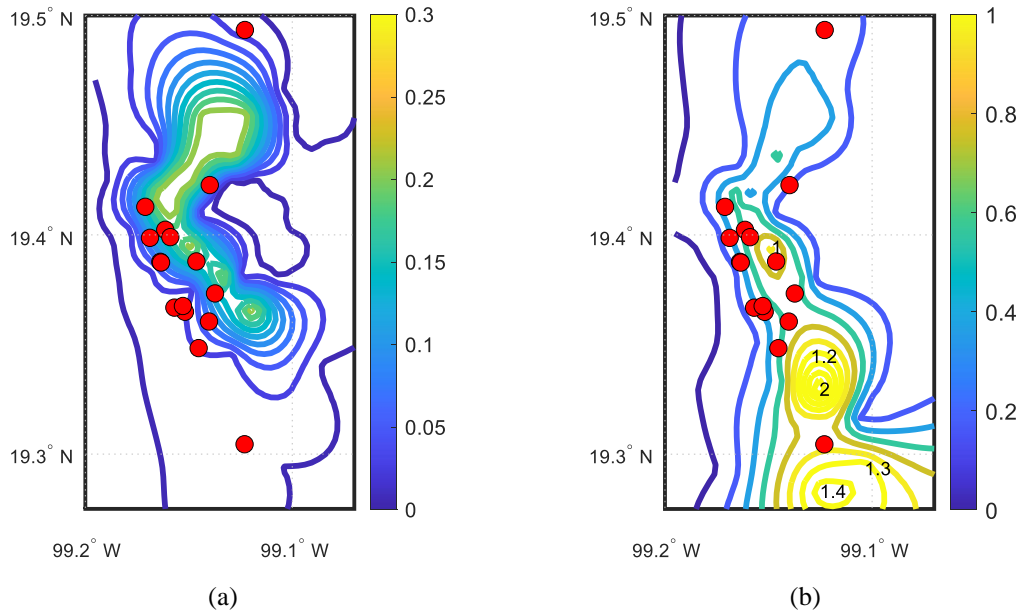


Fig. 16 Prototype iso-damage index curves (low-cycle fatigue model) - (a) 1985, (b) 1985+2017

represents mainly the demand from the SCT station in the N90E direction. In the southern zone, the accumulation of damage from this earthquake is less than 5%. When the joint action of the 1985 and 2017 earthquakes is considered (Fig. 16b), 5 stations reach  $DI > 1$ , which means that practically all the accumulation of fatigue damage occurs in the 2017 earthquake. On the northern side of the city, only the SCT station achieves a  $DI > 1$  ( $DI = 1.01$ ). It is observed that only 2 cases marked in red fall within an isocurve with damage  $DI > 1$ , and 13 of the 16 cases fall within the isocurve associated with a  $DI = 0.4$ , thus the sensitivity of the damage to variations in the structural parameters is evaluated.

First, the axial load is increased by only 5% in the prototype, and the analysis is performed once again (Fig. 17a). On the other hand, the effect of reducing the cross-section of the columns by 5% is evaluated, that is, changing the section width from 500 mm to 475 mm throughout the height of the columns (Fig. 17b). In these analyzes, the black points indicate the stations in which the dynamic analysis (including the 1985 and 2017 records) was not completed due to the lack of convergence in one of the steps. These values are excluded from the analysis. For these cases, the average DI over the 16 collapsed buildings increases from 0.28 for the original model (Fig. 16b) to 0.56 (Fig. 17a) and 0.48 (Fig. 17b), respectively, giving a better correlation with the observed collapsed buildings. The DI level increases, extending the damage zone towards the northern side of the city. In these cases, most of the collapsed buildings fall within the isocurves associated with  $DI = 0.6$ . The increase in the intensity of the isocurves provides damage congruence with 9 of the 16 cases, and having the other 7 cases less than 2 km away (Fig. 17a).

Another relevant comparison is the effect of column strength improvement (considering the 1985 and 2017 records). Thus, increasing the cross-section of all columns in height, from a column width of 500 mm to 600 mm is studied (Fig. 18a). On the other hand, the steel longitudinal ratio of the columns of the first floor is increased, going from 1.2% to 2.0% for another analysis (Fig.

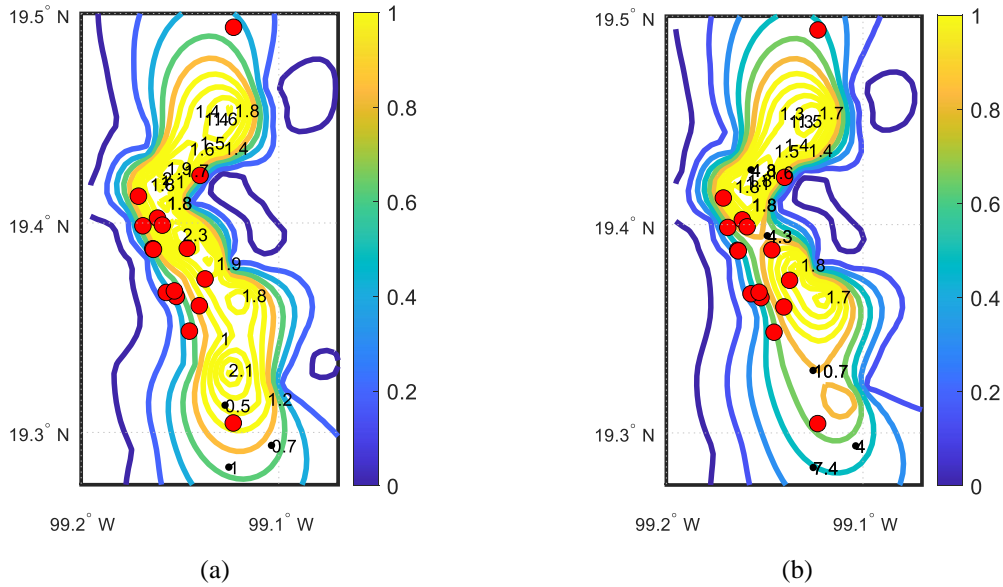


Fig. 17 Iso-damage index curves (1985+2017) - (a) +5% axial load, (b) -5% column width

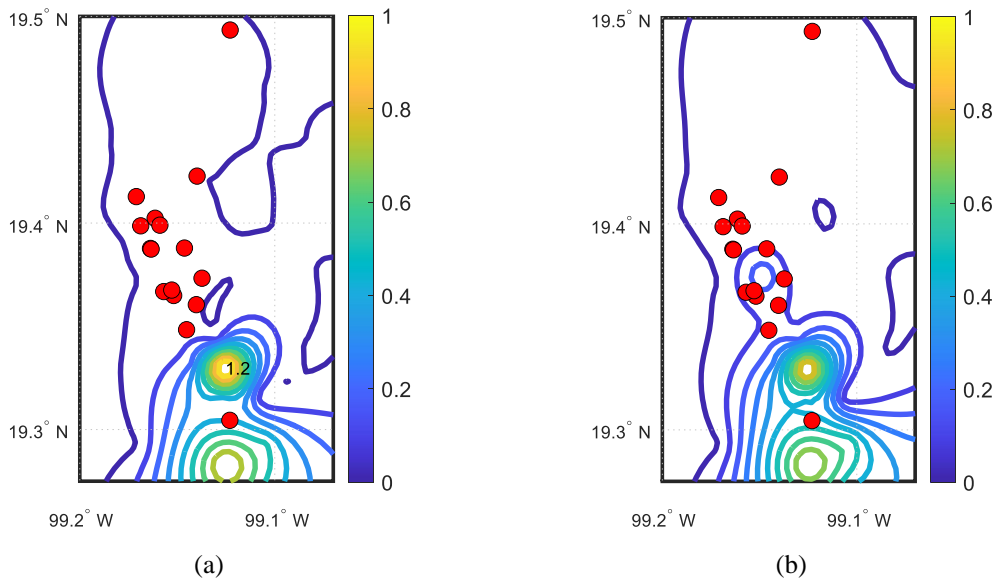


Fig. 18 - Iso-damage index curves (1985+2017) - (a) +20% columns size, (b) 2% steel reinforcing ratio

18b). The average DI for these cases on the collapsed buildings is 0.06 and 0.08, respectively. The northern part of the city does not evidence accumulation of fatigue damage, and only one station imposes the fracture of the reinforcement (Fig. 18a). The distribution and reduced magnitude of the DI isocurves are consistent with Mexican buildings that had more robust columns and were exempt from severe damage after the 2017 earthquake (Albornoz *et al.* 2022).

Finally, the prototype model is evaluated by considering special detailing in the areas of the

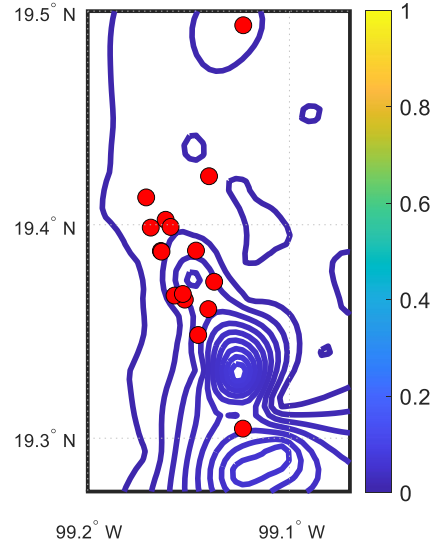


Fig. 19 Iso-damage index curves for a frame with special detailing (1985+2017)

plastic hinge, for both beams and columns (considering the 1985 and 2017 records). In this case, the concrete core is confined and the transversal reinforcement constrains the buckling of the longitudinal bars, such the reinforcing bar does not lose compressive strength. This restricts the slenderness ratio  $L/D$  to a value of 6. In the case of the confined concrete model, given its ductile behavior, the ultimate strain is increased from 0.01 (Fig. 8b) for unconfined concrete to 0.075 for the columns. This case represents those buildings built between the 70s and 80s, which were not damaged in the 2017 or the 1985 events, which were designed with the 1976 design code. This regulation required special detailing on this type of structure. The results are shown in Fig. 19, where the average DI over the collapsed buildings is 0.01, and the most demanding station has a  $DI = 0.06$ . The reduction in slenderness increases considerably the fatigue life, reducing largely the DI values, compared to the observed response with poor detailing in older buildings (Fig. 16b).

## 5.2 Model analysis of SDOF

### (a) Displacement approach

For comparison purposes, the displacement demands of a single degree of freedom (SDOF) system are contrasted with the displacement capacity of the prototype building, as it is usually performed by displacement-based design approaches (e.g., shear wall detailing in ACI 318-19 (2019)). In order to compare the building displacement capacity with an SDOF response, a factor of 1.3 is considered for transforming the displacement response from an SDOF system to an MDOF (multi-degree of freedom) system, such as the prototype building. Considering that a degradation of 20% of the strength of the prototype starts at about 100 mm (Fig. 9), the displacement capacity is reached for an SDOF at about 80 mm ( $\sim 100/1.3$ ), a value that corresponds to isocurves in orange in Figs. 20-21 according to the damage scale color.

Maximum elastic/inelastic displacements are calculated for all stations for an SDOF model. All analyses consider a fundamental cracked period of 1.0 s. Using the same data interpolation

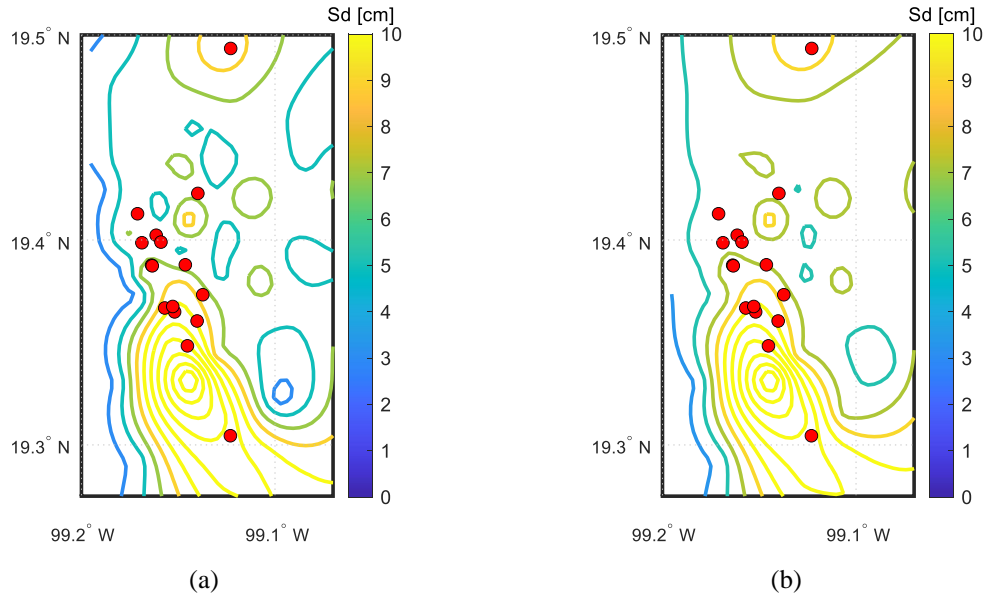


Fig. 20 Elastic displacement demand (Sd) - (a) only 2017, (b) 1985+2017

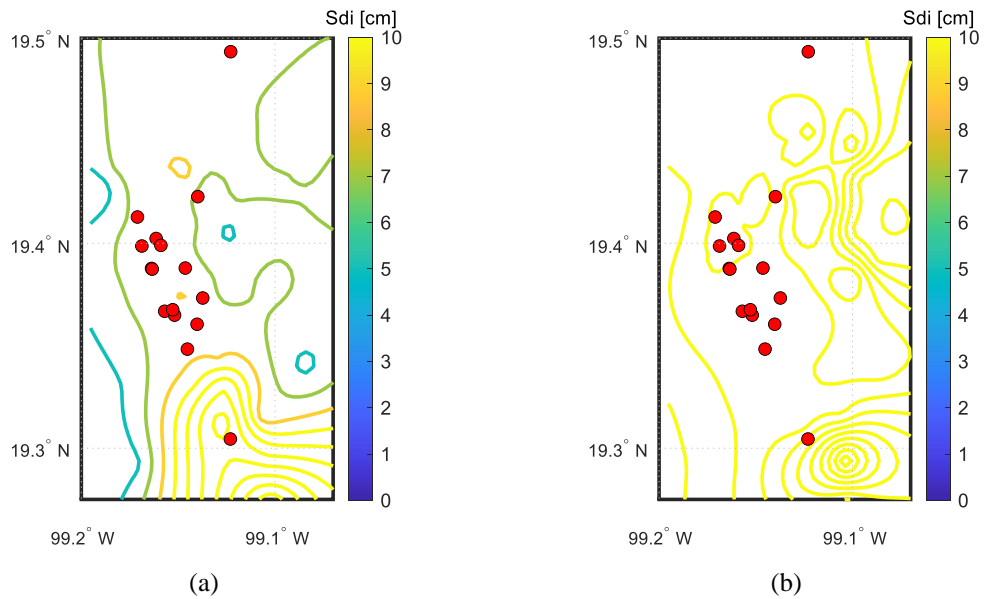


Fig. 21 Inelastic displacement demand (Sdi) for both earthquakes (1985+2017) - (a)  $\Omega=3$ , (b)  $\Omega=1$

methodology, isocurves are generated that represent the same displacement demand level. First, the elastic (Sd, Fig. 20) displacement spectra, considering only the 2017 earthquake and the combination of the 1985 and 2017 earthquakes, are created. The inelastic response (Sdi, Fig. 21) is calculated by fixing the SDOF oscillator strength according to the 1966 design spectrum, for an over-strength  $\Omega = 3$  (Fig. 21a), that is, 3 times the strength of the 1966 code, which is consistent

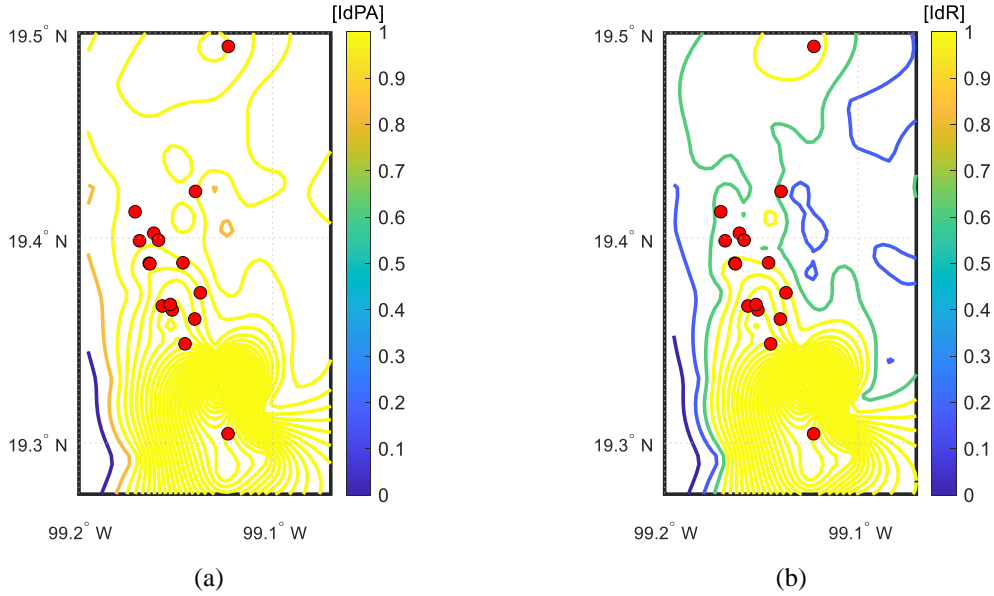


Fig. 22 Damage index (1985+2017) - (a) Park and Ang (1985), (b) Rodriguez (2018) for  $H/T=20$

with the prototype over-strength. An over-strength  $\Omega = 1$  (Fig. 21b) is also included for comparison purposes.

In Fig. 20, it is shown that the elastic demands exceed the capacity of the structure ( $\sim 80$  mm) on the southern side of the city, even when only the 2017 records are considered (Fig. 20a). In general, the northern part of the city does not reach the displacement capacity of the structure for either earthquake, suggesting that other considerations are required, such as damage accumulation. It should be mentioned that, for the elastic spectrum, the consideration of both records (Fig. 20b) results in the envelop spectrum of them.

The inelastic response for the case  $\Omega = 3$  (Fig. 21a), reinforces the previous finding. Higher displacement demands are concentrated in the southern part of the city, while the demands in the northern zone decrease in magnitude, remaining below the capacity of the structure. On the other hand, the inelastic displacement demands for  $\Omega = 1$  exceed the capacity of the structure, covering an area of damage broader than that observed when both records are used (Fig. 21b). Thus, it is unlikely that an over-strength value of  $\Omega = 1$  would have been observed in buildings with the characteristics of the prototype (with reduced strength) in the area.

#### (b) Energy approach

The energy-based damage indexes proposed by Rodriguez (2018) and by Park and Ang (1985) are also studied for both earthquakes combined (1985 and 2017). Other works have used similar approaches, considering local or global response (e.g., Sadeghi and Nouban, 2016; Teran-Gilmore and Jirsa, 2005; Guo and He, 2018; Kang and Lee, 2016). The Park and Ang index ( $D_{PA}$ ) is a well-recognized damage function in the literature. It results from a linear combination between the normalized maximum displacement ( $x_{max}$ ) and dissipated hysteretic energy ( $E_h$ ) (Eq. 4), where the value of  $D_{PA} \geq 1$  means the collapse of the system. The displacement component is controlled by the maximum monotonic capacity associated with a 20% loss of strength ( $x_{u,mon}$ ), that is, when the load is reduced from its peak to  $0.8F_y$ . The contribution of the hysteretic energy

dissipated during the seismic actions is controlled by the factor  $\beta_1$ , which varies between -0.3 and 1.2 with a median value of 0.15 for RC elements (Cosenza *et al.* 1993). Typically, a high  $\beta_1$  value represents a poorly designed (and detailed) structure, commonly observed in old buildings (Cosenza *et al.* 1993). In this study, the value of 0.15 is chosen.

$$D_{PA} = \frac{x_{max}}{x_{u,mon}} + \beta_1 \frac{E_h}{F_y x_{u,mon}} \quad (4)$$

Similar to the spectral displacement, the damage index ( $D_{PA}$ ) is computed for inelastic behavior with a fixed strength according to the 1966 design code with  $\Omega = 3$  (Fig. 22a). In Fig. 22a, it is shown that the index provides a good correlation with the collapsed building locations, although covering a broader area of potential collapsed buildings.

Unlike the Park and Ang model, the Rodriguez model ( $I_d$  - Eq. 5) is a damage index based solely on energy, which was validated using 11 historical earthquakes on RC frame and wall structural systems. It is a coefficient that normalizes the dissipated hysteretic energy ( $E_h$ ) by the energy absorbed in the same system, but with an elastic response ( $E_\lambda$ ). Thus,  $E_\lambda$  depends on the cracked period ( $T_{cr}$ ), the modal participation factor ( $\Gamma$ ), which is assumed as 5/4, the total height of the building ( $H$ ), and the roof drift at the level of potential collapse ( $Drc$ ). The value of  $Drc$  is assumed as 0.5% (Fig. 9), although a value of 2.5% is suggested for buildings that are designed according to modern design codes for earthquake-resistant structures (Rodriguez 2018).

$$I_d = \frac{E_h}{E_\lambda} = \frac{\Gamma^2 E_h}{\left(2\pi \frac{H}{T_{cr}} Drc\right)^2} \quad (5)$$

In this study, the damage index ( $I_d$ ) is computed with  $H/T_{cr} = 19.7\text{m}/1.0\text{s} \sim 20 \text{ m/s}$  and a strength set according to the 1966 design code with  $\Omega = 3$  (Fig. 22b). Similar to the displacement indexes, for  $\Omega = 3$  (Fig. 22b), a good correlation with the collapsed building locations is observed, especially in the southern area, with practically all red points close to an isocurve with  $I_d \sim 0.7$ . Taking into consideration that Eq. (5) is highly dependent on  $H/T_{cr}$  and  $Drc$ , an increase in such factors reduces rapidly the index value. A value of  $H/T_{cr} = 40 \text{ m/s}$  represents rigid buildings such as structures based on RC walls that mostly did not present damage after the 2010 Chile earthquake (Massone *et al.* 2012, Lagos *et al.* 2021). Moreover, proper detailing would also increase the  $Drc=0.5\%$  value, reducing the likelihood of collapse.

## 6. Conclusions

A series of buildings in Mexico City with column damage on the soft first story were reported after the 2017 earthquake. These buildings were commonly built before 1985 and it was common to observe buckling in the longitudinal bars and concrete spalling due to poor detailing. In particular, 16 buildings between 4- and 8-story high presented a collapse mechanism associated with column failure on the first story. The effect of the accumulated damage for the 1985 and 2017 earthquakes that could have generated the collapse of some of these structures was studied in this work. In general, the elastic and inelastic displacement demands registered in different places were shown to be higher in 1985, inferring that the displacement demand does not explain the collapse of all these structures. Moreover, the results suggest that the northern part of the city should have

been affected by other effects than displacement demands, in order to explain the observed damage. The accumulated damage models based on a simplified system (SDOF) provided a good correlation with the observed damage location but concentrated in the southern side of the city. The approach, however, contains a series of limitations that prevent, for example, determining the location or the type of damage in the structure, or providing design tools for design improvement. The present research proposes to measure the accumulated damage in the reinforcement to study the fatigue failure as a potential factor in the collapse of buildings in the 2017 Mexico earthquake.

The damage index of reinforcing steel was determined from a planar prototype building model in all the stations that recorded the 2017 earthquake. The interpolation of data allowed generating damage index isocurves that were contrasted with the location of the 16 cases of collapse under study, obtaining a good correlation when a slight increase (5%) in the axial load or decrease in the cross-section of the columns (5%) was included in the model. Biaxial loading in columns could also increase the damage, although the model is not able to capture such an effect due to its planar nature. The analysis also indicates that increasing the cross-section of the columns by 20% or increasing the ratio of longitudinal reinforcement in columns to 2%, promoted favorable effects on seismic performance that translates into a lower accumulation of low-cycle fatigue damage. Furthermore, adequate detailing (concrete confinement and bar buckling constraint) in columns translates into an even greater improvement. This is largely due to the increase in fatigue life obtained with the decrease in the slenderness of the longitudinal reinforcement from  $L/D = 24$  to 6. This also may explain why buildings from the 70s-80s designed with the 1976 design code, which had special detailing requirements in areas of plastic hinges, did not suffer damage after the 2017 earthquake despite having previously suffered the 1985 earthquake.

## Acknowledgement

The authors would like to thank the Seismic Instrumentation Unit of the Institute of Engineering at National University of Mexico - UNAM (RAII), the “Red Sísmica del Valle de México” (RSVM), belonging to the National Seismological Service and the Center for Instrumentation and Seismic Records (CIRES) for providing the seismic records used in this work, and in particular to Sergio Alcocer, Héctor Guerrero and Miguel Jaimes. Julian Carrillo thanks Vicerrectoría de Investigaciones at Universidad Militar Nueva Granada for providing research grants.

## References

- ACI 318-19 (2019), Building code requirements for structural concrete and commentary (2019), American Concrete Institute, Farmington Hills, Mich.
- Albornoz, T.C., Massone, L.M., Carrillo, J., Hernández, F., Alberto, Y. (2022), “Validation of the seismic response of an RC frame building with masonry infill walls: The case of the 2017 Mexico earthquake”, *Adv. Comput. Des.*, **7**(3), 229-251. <https://doi.org/10.12989/acd.2022.7.229>.
- Arteta, C.A., Carrillo, J., Archbold, J., Gaspar, D., Pajaro, C., Araujo, G., Torregroza, A., Bonett, R., Blandon, C., Fernandez-Sola, L.R., Corral, J.F., Mosalam, K.M. (2019), “Response of midrise reinforced concrete frame buildings to the 2017 Puebla earthquake”, *Earthq. Spectr.*, **35**(4), 1763-1793. <https://doi.org/10.1193/061218EQS144M>.
- CDMX government (2017), Geological Hazard Maps: Seismic Zoning Map, Gobierno de la Ciudad de

- México, Mexico City, Mexico. [http://data.proteccioncivil.cdmx.gob.mx/mapas\\_sgm/mapas\\_sgm2.html](http://data.proteccioncivil.cdmx.gob.mx/mapas_sgm/mapas_sgm2.html).
- Cosenza, E., Manfredi, G., Ramasco, R. (1993), “The use of damage functionals in earthquake engineering: A comparison between different methods”, *Earthq. Eng. Struct. Dyn.*, **22**(10), 855-868. <https://doi.org/10.1002/eqe.4290221003>.
- Dhakal, R.P., Maekawa, K. (2002), “Reinforcement stability and fracture of cover concrete in reinforced concrete members”, *J. Struct. Eng.*, **128**(10), 1253-1262. [https://doi.org/10.1061/\(ASCE\)0733-9445\(2002\)128:10\(1253\)](https://doi.org/10.1061/(ASCE)0733-9445(2002)128:10(1253)).
- Downing, S.D., Socie, D.F. (1982), “Simple rainflow counting algorithms”, *Int. J. Fatigue*, **4**(1), 31-40. [https://doi.org/10.1016/0142-1123\(82\)90018-4](https://doi.org/10.1016/0142-1123(82)90018-4).
- FEMA-356 (2000), “Prestandard and Commentary for Seismic Rehabilitation of Buildings”, Federal Emergency Management Agency, Washington DC, U.S.A.
- Galvis, F.A., Miranda, E., Heresi, P., Dávalos, H., & Ruiz-García, J. (2020), “Overview of collapsed buildings in Mexico City after the 19 September 2017 (Mw7.1) earthquake”, *Earthq. Spectr.*, **36**(2\_suppl), 83-109. <https://doi.org/10.1177/8755293020936694>.
- Google maps (2018), Earthquake of 09/19/2017 in CDMX – Collection of collapsed buildings, Mexico. <https://www.google.com/maps/d/u/0/viewer?mid=18a98CKWjzoleGvBtOnbBVv5D4JA&ll=19.40354823345304%2C-99.13143420597697&z=14>
- Google maps (2017), Mexico City, Mexico. <https://www.google.cl/maps/place/Cd.+de+Mexico,+Mexico/>.
- Guo, X., He, Z. (2018), “Vibration-mode-based story damage and global damage of reinforced concrete frames”, *Earthq. Struct.*, **14**(6), 589-598. <https://doi.org/10.12989/eas.2018.14.6.589>.
- Jiménez, F.J., Massone, L.M. (2018), “Experimental seismic shear force amplification in scaled RC cantilever shear walls with base irregularities”, *Bull Earthq. Eng.*, **16**(10), 4735-4760. <https://doi.org/10.1007/s10518-018-0343-7>.
- Kang, J.W., Lee, J.A. (2016), “New damage index for seismic fragility analysis of reinforced concrete columns”, *Struct. Eng. Mech.*, **60**(5), 875-890. <https://doi.org/10.12989/sem.2016.60.5.875>.
- Kwak, K.H., Park, J.G. (2001), “Shear-fatigue behavior of high-strength reinforced concrete beams under repeated loading”, *Struct. Eng. Mech.*, **11**(3), 301-314. <https://doi.org/10.12989/sem.2001.11.3.301>.
- Lagos, R., Lafontaine, M., Bonelli, P., Boroschek, R., Guendelman, T., Massone, L.M., Saragoni, R., Rojas, F., Yañez, F. (2021), “The quest for resilience - The Chilean practice in seismic design of reinforced concrete buildings”, *Earthq. Spectr.*, **37**(1), 26-45. <https://doi.org/10.1177/8755293020970978>.
- Li, K., Wang, X.L., Cao, S.Y., Chen, Q.P. (2015), “Fatigue behavior of concrete beams reinforced with HRBF500 steel bars”, *Structural Eng. Mech.*, **53**(2), 311-324. <https://doi.org/10.12989/sem.2015.53.2.311>.
- Massone, L.M., Bedecarratz, E., Rojas F., Lafontaine, M. (2021), “Nonlinear modeling of a damaged reinforced concrete building and design improvement behavior”, *J. Build. Eng.*, **41**, 102766. <https://doi.org/10.1016/j.jobe.2021.102766>.
- Massone, L.M., Bonelli, P., Lagos, R., Lüders, C., Moehle, J., Wallace, J.W. (2012), “Seismic design and construction practices for RC structural wall buildings”, *Earthq. Spectr.*, **28**(S1), S245-S256. <https://doi.org/10.1193/1.4000046>.
- Massone, L.M., Herrera, P.A. (2019), “Experimental study of the residual fatigue life of reinforcement bars damaged by an earthquake”, *Mater. Struct.*, **52**(3), 61. <https://doi.org/10.1617/s11527-019-1361-x>.
- Massone, L.M., López, E.E. (2014), “Modeling of reinforcement global buckling in RC elements”, *Eng. Struct.*, **59**, 484-494. <https://doi.org/10.1016/j.engstruct.2013.11.015>.
- Massone, L.M., Moroder, D. (2009), “Buckling modeling of reinforcing bars with imperfections”, **31**, 758-767. <https://doi.org/10.1016/j.engstruct.2008.11.019>.
- Massone, L.M., Ostoic, D.F. (2020), “Shear strength estimation of masonry walls using a panel model”, *Eng. Struct.*, **204**, 109900. <https://doi.org/10.1016/j.engstruct.2019.109900>.
- Matlab (2020), Ordinary kriging Interpolation, MATLAB, USA. <https://www.mathworks.com/matlabcentral/fileexchange/57133-kriging-x-y-z-range-sill>.
- Mayoral, J.M., Castañón, E., Alcantara, L., Tepalcapa, S. (2016), “Seismic response characterization of high plasticity clays”, *Soil Dyn. Earthq. Eng.*, **84**, 174-189. <https://doi.org/10.1016/j.soildyn.2016.02.012>.

- McKenna, F., Fenves, G.L., Scott, M.H., Jeremic, B. (2000) "Open system for earthquake engineering simulation" (OpenSees, Version 2.4.3), Pacific Earthquake Engineering Research Center, University of California, California, U.S.A.
- Meli, R., Reyes, A. (1971), "Mechanical properties of masonry", School of Engineering, UNAM, Mexico.
- Muriá Vila, D., González Alcorta, R. (1995), "Dynamic properties of buildings in Mexico City", *Revista de Ingeniería Sísmica*, **51**, 25-45.
- NCR (1966), "New Construction Regulations of the Federal District (1966)", México.
- NTC (2017), "Complementary Technical Standards for Earthquake Design", Official Gazette of the Federal District, Mexico City, Mexico.
- NTC-C (1976), "Complementary Technical Standards for Design and Construction of Concrete Structures", Official Gazette of the Federal District, Mexico City, Mexico.
- NTC-S (1976), "Complementary Technical Standards for Earthquake Design", Official Gazette of the Federal District, Mexico City, Mexico.
- Ozkaynak, H., Yuksel, E., Yalcin, C., Dindar, A.A., Buyukozturk, O. (2014), "Masonry infill walls in reinforced concrete frames as a source of structural damping of structural damping", *Earthq. Eng. Struct. Dyn.*, **43**, 949-968. <https://doi.org/10.1002/eqe.2380>.
- Park, Y.J., Ang, A.H.S. (1985), "Mechanistic seismic damage model for reinforced concrete", *J. Struct. Eng.*, **111**(4), 722-739. [https://doi.org/10.1061/\(ASCE\)0733-9445\(1985\)111:4\(722\)](https://doi.org/10.1061/(ASCE)0733-9445(1985)111:4(722)).
- Quintanar, L., Cárdenas-Ramírez, A., Bello-Segura, D.I., Espíndola, V.H., Pérez-Santana, J.A., Cárdenas-Monroy, C., Carmona-Gallegos, A.L., Rodríguez-Rasilla, I. (2018), "A Seismic Network for the Valley of Mexico: Present Status and Perspectives", *Seismol. Res. Lett.*, **89**(2A), 356-362. <https://doi.org/10.1785/0220170198>.
- Rodríguez, M., Botero, J. (1996), "Aspects of the seismic behavior of reinforced concrete structures considered mechanical properties of reinforcement steel produced in Mexico", UNAM, II, 575.
- Rodríguez, M.E. (2018), "Damage index for different structural systems subjected to recorded earthquake ground motions", *Earthq. Spectr.*, **34**(2), 773-793. <https://doi.org/10.1193/021117EQS027M>.
- Rodríguez, M.E. (2020), "The interpretation of cumulative damage from the building response observed in Mexico City during the 19 September 2017 earthquake", *Earthq. Spectr.*, **36**(2\_suppl), 199-212. <https://doi.org/10.1177/8755293020971307>.
- Sadeghi, K., Nouban, F. (2016), "Damage and fatigue quantification of RC structures", *Struct. Eng. Mech.*, **58**(6), 1021-1044. <https://doi.org/10.12989/sem.2016.58.6.1021>.
- Teran-Gilmore, A., Jirsa, J.O. (2005), "A damage model for practical seismic design that accounts for low cycle fatigue", *Earthq. Spectr.*, **21**(3), 803-832. <https://doi.org/10.1193/1.1979500>.
- Tripathi, M., Dhakal, R.P., Dashti, F., Massone, L.M. (2018), "Low-cycle fatigue behaviour of reinforcing bars including the effect of inelastic buckling", *Constr. Build. Mater.*, **190**, 1226-1235. <https://doi.org/10.1016/j.conbuildmat.2018.09.192>.
- Welt, T.S., Massone, L.M., LaFave, J.M., Lehman, D.E., McCabe, S.L., Polanco, P. (2017), "Confinement behavior of rectangular reinforced concrete prisms simulating wall boundary elements", *J. Struct. Eng. ASCE*, **143**(4), 04016204. [https://doi.org/10.1061/\(ASCE\)ST.1943-541X.0001682](https://doi.org/10.1061/(ASCE)ST.1943-541X.0001682).